Available online at BCREC website: https://bcrec.id

Bulletin of Chemical Reaction Engineering & Catalysis, 16 (2) 2021, 320-330

Research Article

Cellulose and TiO_2–ZrO_2 Nanocomposite as a Catalyst for Glucose Conversion to 5-EMF

F.W. Dini, H. Helmiyati*), Y.K. Krisnandi

Department of Chemistry, Faculty of Mathematics and Natural Sciences, Universitas Indonesia, Depok 16424, West Java, Indonesia.

Received: 8th February 2021; Revised: 15th April 2021; Accepted: 16th April 2021
Available online: 18th April 2020; Published regularly: June 2021

Abstract

This work demonstrated the use of green material catalysts, produced from *Sengon* sawdust waste, to obtain nanocellulose biopolymers. The green material catalysts were utilized as catalysts support of TiO_2–ZrO_2 binary oxide in the form of nanocomposite materials with superior synergistic properties. The isolation of nanocellulose was achieved using a hydrolysis method with a yield of 63.40%. The TiO_2 and ZrO_2 nanoparticles have average particle sizes of around 25 and 15 nm, respectively, and the binary oxides of TiO_2–ZrO_2 pretained an average particle size of 30 nm were used. Furthermore, the nanocellulose combined with the TiO_2–ZrO_2 binary oxide had formed a cellulose/TiO_2–ZrO_2 nanocomposite with an average particle size of 30 nm. This indicates that the supporting nanocellulose can stabilize the nanoparticles and avoid aggregation. Moreover, the nanocomposites can be used as a catalyst for the conversion of glucose to 5-ethoxymethylfurfural (5-EMF). The catalytic activity increased with the nanoparticle effect obtained ZrO_2, TiO_2, TiO_2-ZrO_2, and cellulose and TiO_2-ZrO_2 nanocomposite, in 15.50%, 20.20%, 35.20%, and 45.50% yields, respectively. The best yield of 5-EMF was 45.50%, with reaction conditions of 1:1 TiO2–ZrO2 ratio, 4 h reaction time, and 160 °C reaction temperature. The use of nanocellulose biopolymer generated from *Sengon* sawdust waste in Indonesia provides a promising catalyst support material as an alternative green catalyst. In addition, the glucose carbohydrates can be converted to biofuel feedstocks in the development of a renewable alternative energy.

Keywords: Catalyst; Glucose; Nanocellulose; Nanocomposite; 5-ethoxymethylfurfural

How to Cite: F.W. Dini, H. Helmiyati, Y.K. Krisnandi (2021). Cellulose and TiO_2–ZrO_2 Nanocomposite as a Catalyst for Glucose Conversion to 5-EMF. *Bulletin of Chemical Reaction Engineering & Catalysis*, 16(2), 320-330 (doi:10.9767/bcrec.16.2.10320.320-330)

Permalink/DOI: https://doi.org/10.9767/bcrec.16.2.10320.320-330

1. Introduction

The development of nanotechnology and nanomaterials contribute to the research and opportunities in various industrial sectors. The application of nanotechnology makes it possible to use forests as a potential platform for bioproducts. The industrial activity of forest processing produces roughly 180 million m^3 of lignocellulose residues, such as sawdust, and other wood wastes [1]. Sawdust accounts for 75 million m^3 of wood waste globally. It is mainly composed of 61.2% cellulose, 25.6% lignin, 9.3% extractive, and 3.9% ashes [2]. The sawdust is often disposed of into rivers or directly burned despite the serious environmental pollution caused by the process [3]. Therefore, the utilization of sawdust waste as a source of cellulose can reduce the environmental impact of its disposal.

* Corresponding Author.
Email: helmiyati@sci.ui.ac.id (H. Helmiyati);
Telp: +62-21-7210027, Fax: +62-21-7863432

Cellulose is a biodegradable, biocompatible, nontoxic, porous material and is an abundant biopolymer in nature [4]. It can be converted to nanocellulose and combined with inorganic nanoparticles to produce a nanocomposite with a synergistic character [5]. A nanocomposite of metal oxides supported by biopolymers can potentially facilitate the development of heterogeneous catalysts [6]. In processes requiring high yield and purity, heterogeneous catalysts can replace homogeneous ones owing to their ability to easily separate from the product [7]. The heterogeneous catalysts that were conventionally used include inorganic substances, such as: Fe_3O_4, CaO, Al_2O_3, TiO_2, ZrO_2, and MgO [5,8], in which the TiO_2 and ZrO_2 have excellent acid-base site properties and were good choices as catalysts [9]. The nanocomposite combination of TiO_2 and ZrO_2 can increase the catalytic activity due to their strong interaction, which induces the formation of a new catalytic site [10].

Multiple researchers have extracted cellulose from natural biomass wastes, such as: rice husks [11], rice straws [12,13], grasses [14], pineapple crowns [15], and corncobs [16]. Other research on the application of biocatalysts includes the application of nanocomposite catalysts, such as: cellulose–TiO_2 used for the rapid adsorption of Pb^{2+} [17], CMC–ZrO_2 applied in the fields of ceramics and catalysis [18], cellulose–Fe_3O_4 used for the synthesis of pyranopyrimidine derivatives [19], sodium alginate–TiO_2 utilized for the synthesis of 5-hydroxymethylfurfural (5-HMF) from fructose [20], and calcium alginate–TiO_2–SiO_2 used for the conversion of glucose to 5-HMF [21].

With the depletion of crude oil resources, there is an increasing urgency to convert natural resources to renewable fuels [22]. The 5-EMF compound is one of the derivative compounds of HMF [23]. 5-EMF is believed to be a promising fuel candidate as it has a high energy density of 8.7 kWh/L, which is close to the energy density of gasoline (8.8 kWh/L) and diesel (9.7 kWh/L) and higher than that of ethanol (6.1 kWh/L) [24].

Although many researchers have focused on the synthesis of inorganic nanoparticle-based catalysts for various applications. However, there are limited study focused on the use of nanocellulose from *Sengon* wood saw waste which is widely available in Indonesia as a catalyst support and evaluating the effect of bimetal TiO_2-ZrO_2 on the synthesis of 5-EMF. Nowadays, the production of 5-EMF with a high yield can be achieved through the etherification of 5-HMF. However, the direct use of HMF as a raw material is problematic owing to its high cost [25].

To bridge this gap, this study investigated the effect of the bimetallic TiO_2–ZrO_2 active site on nanocellulose during the synthesis of 5-EMF from glucose, which is renewable and available naturally. Therefore, this research aimed to use glucose as a precursor to produce 5-EMF by incorporating cellulose from *Sengon* sawdust waste into TiO_2–ZrO_2 binary oxide to increase catalytic activity.

2. Materials and Methods

2.1 Materials

Sengon sawdust from Bengkulu, Indonesia, was used as a source of cellulose biopolymer, 97% titanium isopropoxide (TIP) (Merck and Co.) as a nanoparticle synthesis precursor of TiO_2, zirconium(IV) oxychloride octahydrate ($ZrOCI_2.8H_2O$) (Merck and Co.) as a nanoparticle synthesis precursor of ZrO_2, sodium hydroxide (NaOH) (Merck and Co.) as a delignification agent for the removal of hemicellulose, hydrogen peroxide (H_2O_2) (Merck and Co.) as a bleaching agent, sulfuric acid (H_2SO_4) (Merck and Co.) as a hydrolyzer agent, distilled water, ethanol, and dimethyl sulfoxide (DMSO) (Merck and Co.) as solvents, ammonia (NH_4OH) (Merck and Co.) as a base source, and glucose (Merck and Co.) as a precursor of 5-ethoxymethylfurfural synthesis.

2.2 Cellulose Isolation from *Sengon* Sawdust

Cellulose was isolated using a previously reported chemical hydrolysis method with a slight modification [2,16]. The sawdust was washed, dried, and mashed *via* a ball milling process. The first stage involves the delignification process and hemicellulose deletion using 2% NaOH. Then, the sawdust mixture was soaked for 4 h with constant stirring at 80 °C. The second stage involves the bleaching process in which 16% H_2O_2 and 5% NaOH was mixed for 90 min at 55 °C and then filtering and washing of the precipitation with Aqua Dest. The last stage involves the conversion of the precipitate to nanocellulose for a 2-h ultrasound-assisted acid hydrolysis in 45 wt% H_2SO_4 at 45 °C. The obtained nanocellulose precipitate was washed with water to a neutral pH, separated, and then dried.

2.3 Synthesis of Titanium Dioxide (TiO_2)

TiO_2 nanoparticle synthesis was conducted *via* a previously reported sol–gel method with a

slight modification [26]. About 15 mL of TIP was added to 60 mL of ethanol, and the solution was mixed using a magnetic stirrer for 30 min. Distilled water (10 mL) was slowly added to the mixture to achieve the hydrolysis reaction: a white gel was obtained, which was dried at 100 °C and calcined at 450 °C for 2 h.

2.4 Synthesis of Zirconium Dioxide (ZrO_2)

ZrO_2 nanoparticle synthesis was conducted using a previously reported co-precipitation method with a slight modification [27]. $ZrOCI_2.8H_2O$ was dissolved in distilled water, to which a 2 M NaOH solution was added to reach a pH of 10; the solution was slowly stirred for 1 h. The precipitation was filtered and washed with distilled water to neutral pH. Subsequently, it was dried at 60 °C for 24 h and calcined at 700 °C for 1 h.

2.5 Synthesis of TiO_2–ZrO_2

TiO_2–ZrO_2 synthesis was conducted using a previously reported solid-state dispersion method with a slight modification [28]. TiO_2 and ZrO_2 (1:3, 1:1, 3:1) were mixed using ethanol in mortar, and the solvent was removed *via* evaporation. Then, the solution was dried at 110 °C and calcined at 450 °C for 6 h to obtain TiO_2–ZrO_2 binary oxide catalysts.

2.6 Synthesis of Cellulose–TiO_2–ZrO_2 Nanocomposite

Cellulose–TiO_2–ZrO_2 nanocomposite synthesis was conducted using a previously reported impregnation method with a slight modification [29]. First, 2% cellulose was stirred overnight at 80 °C. Then, 75 mL of 2% cellulose was added to 25 mL of TiO_2–ZrO_2 catalyst at room temperature under constant stirring; 25% NH_4OH ammonia was also added to reach a pH of 10. The solution was kept overnight in an oven at 60 °C and washed with distilled water; then, it was centrifuged at 8000 rpm for 10 min and oven-dried at 80 °C for 8 h to obtain cellulose–TiO_2–ZrO_2 nanocomposite.

2.7 Catalysts Characterizations

Fourier transform infrared (FTIR) spectra were analyzed using a Shimadzu IRPrestige-21 instrument in the wavenumber range of 4000–500 cm^{-1}. X-ray diffraction (XRD) was measured using a PANanalytical X-ray diffractometer with a Cu–Kα radiation source at 40 kV and 30 mA and at 2θ from an angle of 0–80°. The morphological analysis was conducted using a JEOL JSM6100 scanning electron microscope (SEM). Transmission electron microscopy (TEM) was measured using a Tecnai 200 kV D2360 SuperTwin instrument.

2.8 Catalytic Activity Evaluation

The catalytic activity of glucose conversion to 5-EMF was evaluated with reference to a previous study with a slight modification [30]. Glucose precursor (100 mg) and nanocellulose–TiO_2–ZrO_2 (20 mg) were added to 5 mL of DMSO solution under stirring at various temperatures (140°C, 160°C, and 180 °C) and reaction times (2, 4, and 6 h). Afterwards, the reaction was stopped using an ice bath. The 5-EMF was determined *via* high-performance liquid chromatography (HPLC) using a UV detector at a wavelength of 285 nm and the C18 column (specific surface area, 330 m^2/g; pore size, 120 Å; carbon content, 16%) at 30 °C with methanol–water (80:20) as a mobile phase and a flow rate of 1 mL per minute. The 5-EMF yield was calculated as follows [31]:

$$EMF\ Yield\ (\%) = \frac{moles\ of\ EMF}{moles\ of\ glucose} \quad (1)$$

3. Results and Discussion

3.1 Nanocellulose from *Sengon* Sawdust

Hydrolysis of *Sengon* sawdust cellulose was performed using a strong acid (H_2SO_4) for the formation of nanocellulose to increase the active group, surface area, and catalytic activity. The nanocellulose obtained was white, similar to pure nanocellulose with a yield of around 63.40%. The cellulose yield was obtained using the source of cellulose biomass and the synthesis method [32,33]. Figure 1 presents the FTIR

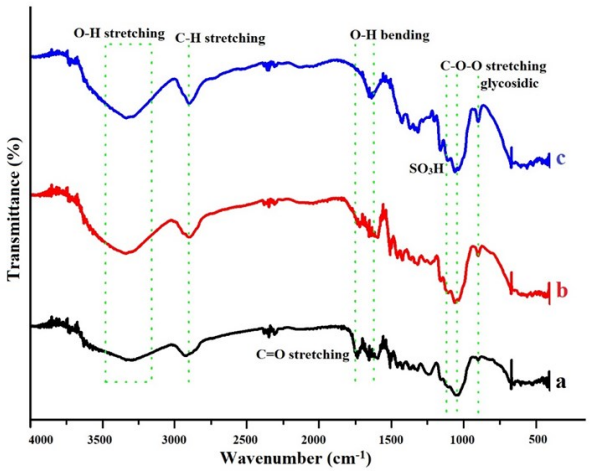

Figure 1. FTIR spectra of (a) *Sengon* sawdust, (b) nanocellulose, and (c) pure nanocellulose.

spectrum of the *Sengon* sawdust, nanocellulose, and pure nanocellulose; there are several of the same absorption bands on the wavenumbers 3200–3400 cm^{-1} (O–H stretching vibration from hydroxyl groups), 2860 cm^{-1} (C–H stretching vibration), and 1659 cm^{-1} (O–H bending vibration). Figure 1a presents the spectrum of the *Sengon* sawdust demonstrating a C=O stretch at 1730 cm^{-1}. Carbonyl is the specific functional group for the lignin due to the wood or the lignocellulosic biomass being primarily composed of cellulose, hemicellulose, and lignin, in which cellulose is covered by lignin and hemicellulose [34].

The lignin peak was not observed in the spectrum of nanocellulose (Figure 1b) and pure nanocellulose (Figure 1c). The spectrum of nanocellulose in Figure 1b shows a specific cellulose absorption band representing the β glycosidic bond C_1–O–C_4 at 800 cm^{-1} and C–O–C stretch at 1082 cm^{-1}. Nanocellulose hydrolysis was conducted using sulfuric acid. A peak was observed at 1035 cm^{-1}, which represents a SO_3^- symmetric vibration; moreover, at 1170 cm^{-1}, a symmetric vibration of an O=S=O unit in the SO_3H group was observed. At 1350 cm^{-1}, there was an asymmetric vibration of SO^{2-}, which is a sulfonate group which becomes the acidic site of the catalyst when is used as a catalyst support.

Figure 2a presents the surface morphology of the *Sengon* sawdust *via* SEM. It can be observed that the surface of the *Sengon* sawdust is thick and has rough lumps as it still contains lignin, hemicellulose, and other impurities. Figure 2b presents the surface morphology of the nanocellulose. From the figure, it can be observed that the nanocellulose has a fiber-like shape and a smooth surface, almost similar to that of pure cellulose (Figure 2c), which has a small fiber size. The results of the SEM support the successful isolation of cellulose from the *Sengon* sawdust.

The XRD pattern of the *Sengon* sawdust (Figure 3a) shows a peak at 2θ = 17.14° and 22.74°. This indicates that the *Sengon* sawdust cellulose is covered by lignin and hemicellulose. The diffraction pattern of nanocellulose (Figure 3b) shows peaks at 2θ = 15.11°(101), the amorphous intensity; 22.49° (002), the maximum intensity; and 34.47° (400). The diffraction pattern of pure cellulose shows peaks at 2θ =15.61°, 22.49°, which was the maximum intensity, and 34.72°. This result is similar to that of a previous study [2]. The XRD pattern shows the crystallinity index based on the maximum intensity and amorphous intensity values. The crystallinity index obtained is 51.16%, which demonstrates a semicrystalline structure.

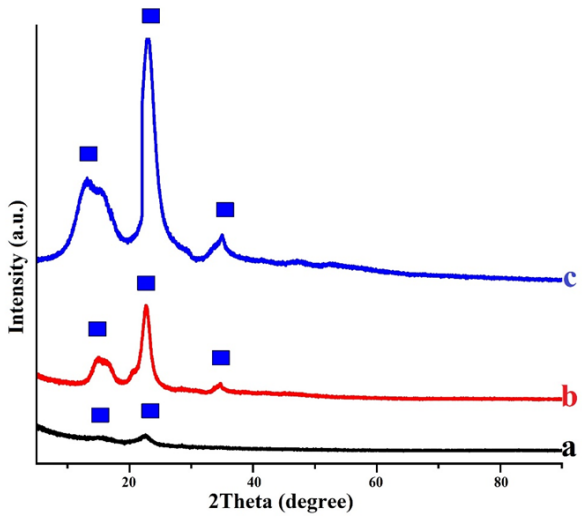

Figure 3. XRD pattern of (a) *Sengon* sawdust, (b) nanocellulose, and (c) pure nanocellulose.

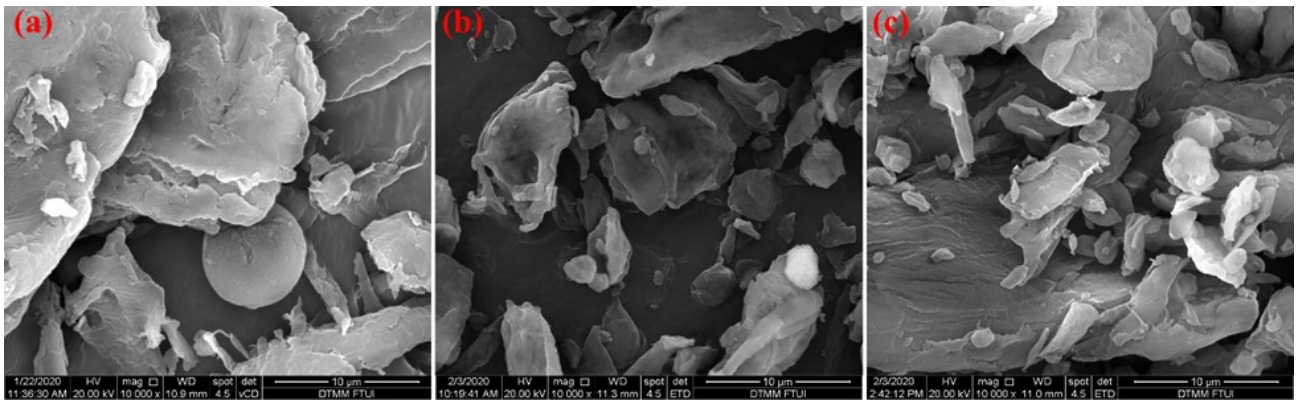

Figure 2. SEM micrographs with ×10.000 magnification. (a) *Sengon* sawdust, (b) nanocellulose, and (c) pure nanocellulose.

3.2 Cellulose–TiO_2–ZrO_2 Nanocomposite

Nanocellulose from *Sengon* sawdust is composed of binary oxide TiO_2–ZrO_2 that forms nanocomposites used as catalysts. Figure 4 presents the FTIR spectra of nanocellulose, TiO_2–ZrO_2, and cellulose–TiO_2–ZrO_2 nanocomposite.

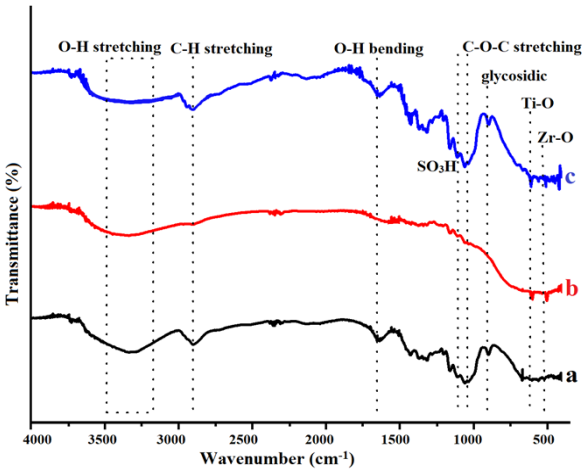

Figure 4. FTIR spectra of (a) nanocellulose, (b) TiO_2–ZrO_2, and (c) cellulose–TiO_2–ZrO_2 nanocomposite.

Figure 4b presents the TiO_2–ZrO_2 spectrum that demonstrates the presence of a weak absorption band at 600 cm^{-1}, which represents the vibration of the Ti–O–Ti bond of the octahedral TiO_6, and the absorption band at 500 cm^{-1}, which represents the vibration of the Zr–O bond. Figure 4c presents the FTIR spectrum of cellulose–TiO_2–ZrO_2 nanocomposites at 3200–3400 cm^{-1}, showing the O–H stretch vibrations of the hydroxyl group, which can be observed due to a decrease in the vibration intensity of the hydroxyl group compared with nanocellulose (Figure 4a). This is due to the strong hydrogen bond between the bimetal and hydroxyl groups in nanocellulose [28]. A C–H stretch is observed at 2860 cm^{-1}, an O–H bend at 1659 cm^{-1}, a β glycosidic bond (C_1–O–C_4) at 800 cm^{-1}, and a C–O–C stretch at 1082 cm^{-1}. Moreover, a Ti–O–Ti bend is observed at 600 cm^{-1} and a Zr–O bend at 500 cm^{-1} at a peak

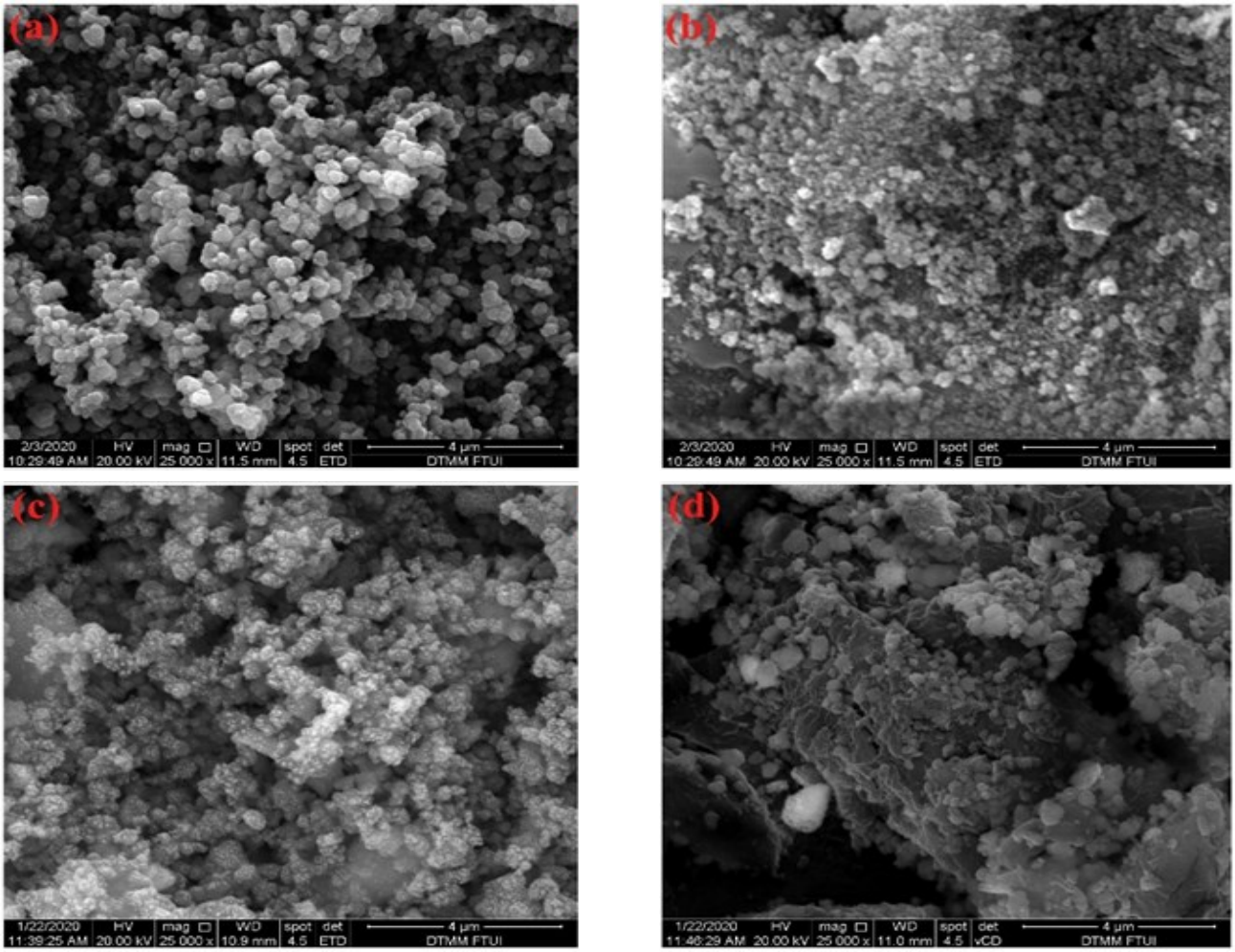

Figure 5. SEM micrograph with ×100.000 magnification. (a) TiO_2, (b) ZrO_2, (c) TiO_2–ZrO_2, and (d) cellulose–TiO_2–ZrO_2 nanocomposite.

shift in a nanocomposite. This supports the successful synthesis of the cellulose–TiO_2–ZrO_2 nanocomposite.

The SEM micrograph in Figure 5a presents the surface morphology of a small spherical TiO_2 surface with a uniform particle size. These results are in accordance with those of a previous study [26]. Figure 5b presents the morphology of ZrO_2, clearly indicating that the form of the granules is not uniform. Figure 5c demonstrates that the surface morphology of TiO_2–ZrO_2 is exhibiting diffused particles of larger sizes. This is due to TiO_2–ZrO_2 combining with a composite form. Figure 5d shows that the cellulose–TiO_2–ZrO_2 nanocomposite can be observed as irregularly shaped TiO_2–ZrO_2 particles embedded in the surface and pores and evenly distributed in the nanocellulose. This shows that the nanocellulose acting as a supporting material has pores (Figure 2b), enabling the active site of TiO_2–ZrO_2 to attach to the surface of the cellulose.

SEM-EDS analysis was conducted to determine the mass percent of each element in the synthesized compound, as presented in Figure 6. The compositions of C, O, Ti, and Zr are 47.2, 39.6, 6.7, and 6.5 wt%, respectively, indicating that the nanocomposite was successfully modified by the bimetal consisting of TiO_2 and ZrO_2, which spread evenly on the surface of the cellulose. This is supported by the results of the surface morphology of obtained via SEM in Figure 5.

Figure 7 presents the XRD pattern of TiO_2–ZrO_2 at 2θ = 25.379°; 30.309°; 35.139°; 50.513°; 60.172°, 62.879° are TiO_2 anatase (in accordance with the JCPDS No. 021-1272) and ZrO_2 tetragonal (in accordance with the JCPDS 080-0965). The XRD pattern of the cellulose–TiO_2–ZrO_2 nanocomposite can be observed at 2θ = 15.101° and 22.748°, which are two specific peaks of nanocellulose and peaks of TiO_2 and ZrO_2 occurred the peak shift. This indicates that TiO_2–ZrO_2 has been successfully combined with a nanocellulose support material.

The XRD pattern can also provide information on the crystal size calculated using the Scherrer equation in Equation (2) [13]:

$$D = \frac{0.9\lambda}{\beta_{1/2}\cos\theta} \quad (2)$$

where D denotes the crystal size; λ, the wavelength (1.406 Å); θ, the diffraction angle; and $\beta_{1/2}$, the full width at half maximum (FWHM). The crystal size of TiO_2–ZrO_2 was 11.86 nm, and the cellulose–TiO_2–ZrO_2 nanocomposite was obtained at 30.42 nm.

A TEM micrograph presents the TiO_2 and ZrO_2 nanoparticles with average particle sizes of around 25 and 15 nm, respectively (Figure 8a and 8b). When these two particles are composited, obtained average particle size were obtained around 30 nm with uniform shape (Figure 8c). The binary oxide is composited with the support material of nanocellulose to form the cellulose–TiO_2–ZrO_2 nanocomposite.

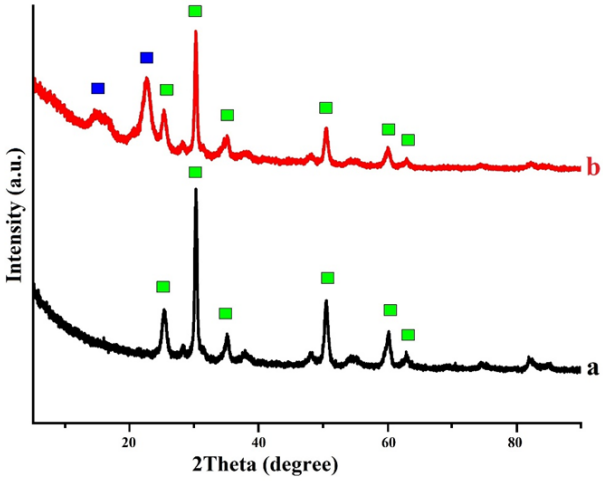

Figure 7. XRD pattern of (a) TiO_2–ZrO_2 and (b) the cellulose–TiO_2–ZrO_2 nanocomposite.

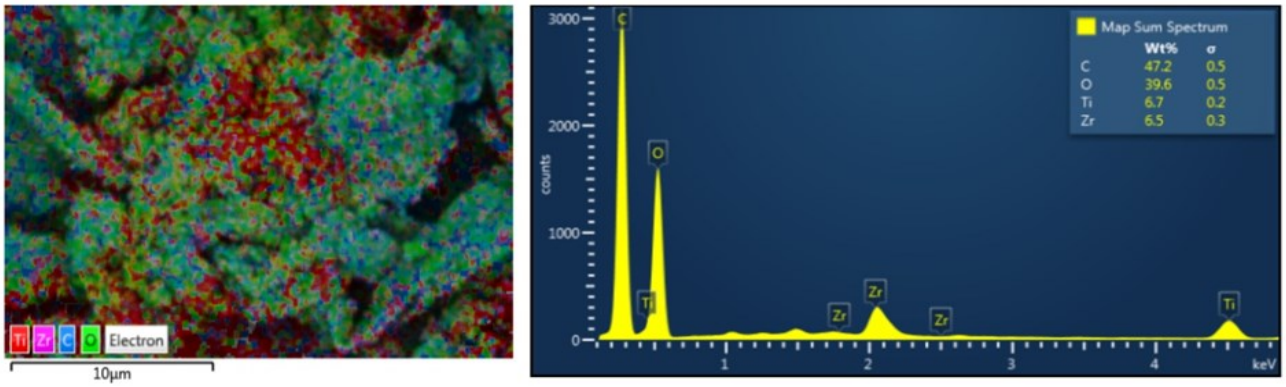

Figure 6. SEM-EDS of the cellulose–TiO_2–ZrO_2 nanocomposite.

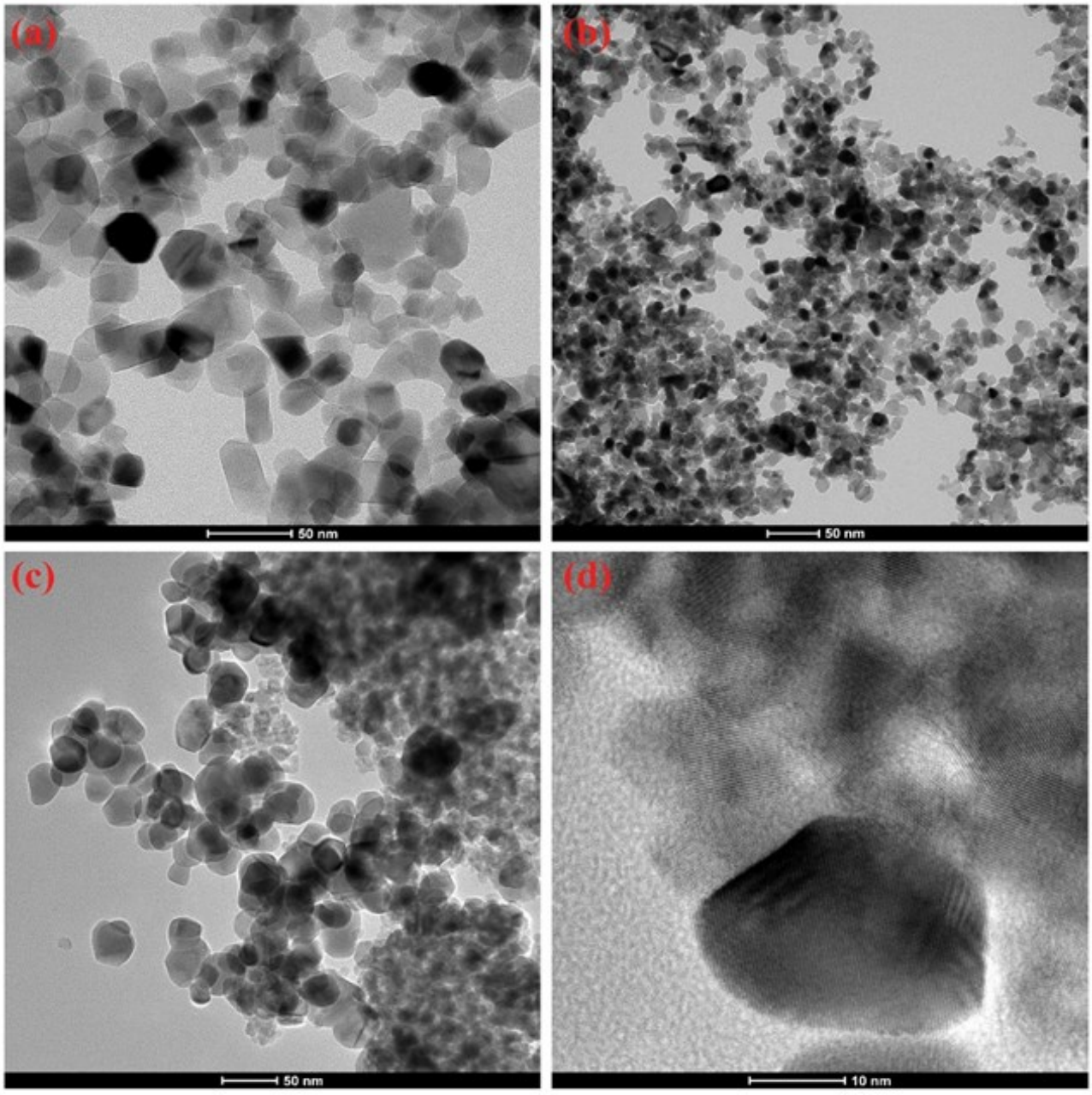

Figure 8. TEM micrographs of (a) TiO_2, (b) ZrO_2, (c) TiO_2–ZrO_2 at a scale of 50 nm, and (d) cellulose–TiO_2–ZrO_2 nanocomposite at a scale of 10 nm.

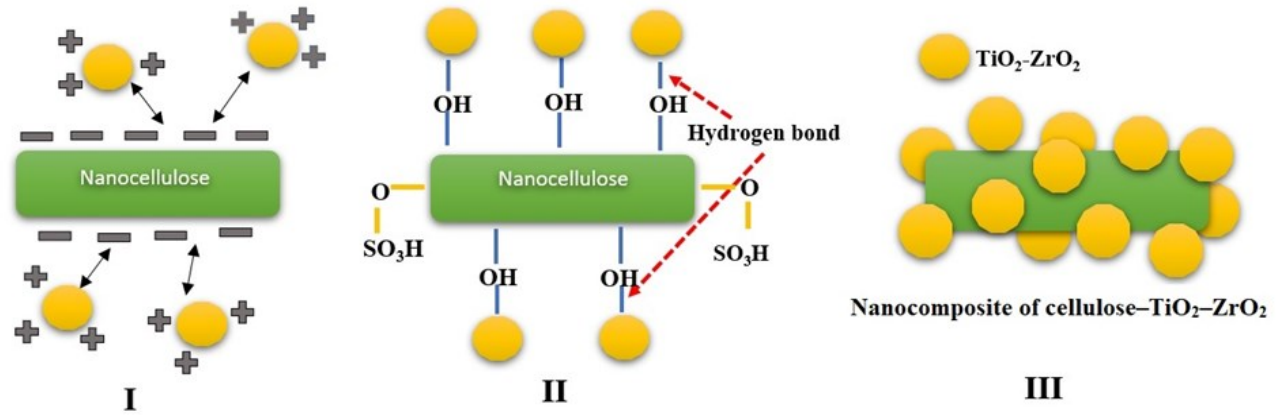

Figure 9. Proposed mechanism of interaction between the nanocellulose and TiO_2–ZrO_2.

The obtained TiO_2–ZrO_2 average particle size was around 30 nm (Figure 8d). This result was supported by the crystal size represented by the XRD pattern.

The proposed mechanism of interaction between cellulose and TiO_2–ZrO_2 is presented in Figure 9. At the first stage (I), TiO_2–ZrO_2 particles with nanocellulose attract each other due to an electrostatic force. In the second stage (II), is formed of hydrogen bonds which can cause a powerful adhesion between the particles. The formation of hybrid particles occurs as long as the surface of the cellulose is filled with sufficient particle layers of TiO_2–ZrO_2 (stage III). If there are no longer free particles of TiO_2–ZrO_2, the surface of the cellulose will be closed partially [35].

3.3 Catalytic Activity of Cellulose–TiO_2–ZrO_2

This work investigated various criteria, namely, the TiO_2–ZrO_2 ratio, reaction time, reaction temperature, and catalyst type. Figure 10a presents the highest percentage of yield product (~43.1%) with the TiO_2–ZrO_2 ratio (1:1) in the catalyst. This yield is obtained due to the synergistic effect of binary oxide that provides an active site to increase the catalytic activity. By using a TiO_2–ZrO_2 ratio of 1:1, the optimum reaction time was 4 h (Figure 10b), with a 5-EMF yield of 45.50%. In addition, when the reaction time increased to 6 h, no significant difference in the yield was observed. By using the optimum conditions of TiO_2–ZrO_2 ratio and reaction time of 4 h, the optimum reaction temperature was 160 °C, with a 5-EMF yield of 45.50% (Figure 10c). When the reaction temperature was increased to 180 °C, the product yield percentage decreased. This is due to the possibility formed insoluble humin by-products [32]. Next, we investigated the effect of the catalyst type on the 5-EMF yield using a TiO_2–ZrO_2 ratio of 1:1 as well as reaction time and reaction temperature of 4 h and 160 °C, respectively. The catalyst type of ZrO_2, TiO_2,

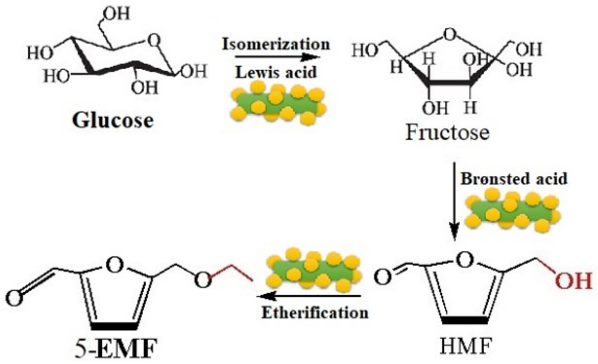

Figure 11. Proposed reaction mechanism of glucose conversions to 5-EMF with a cellulose–TiO_2–ZrO_2 catalyst.

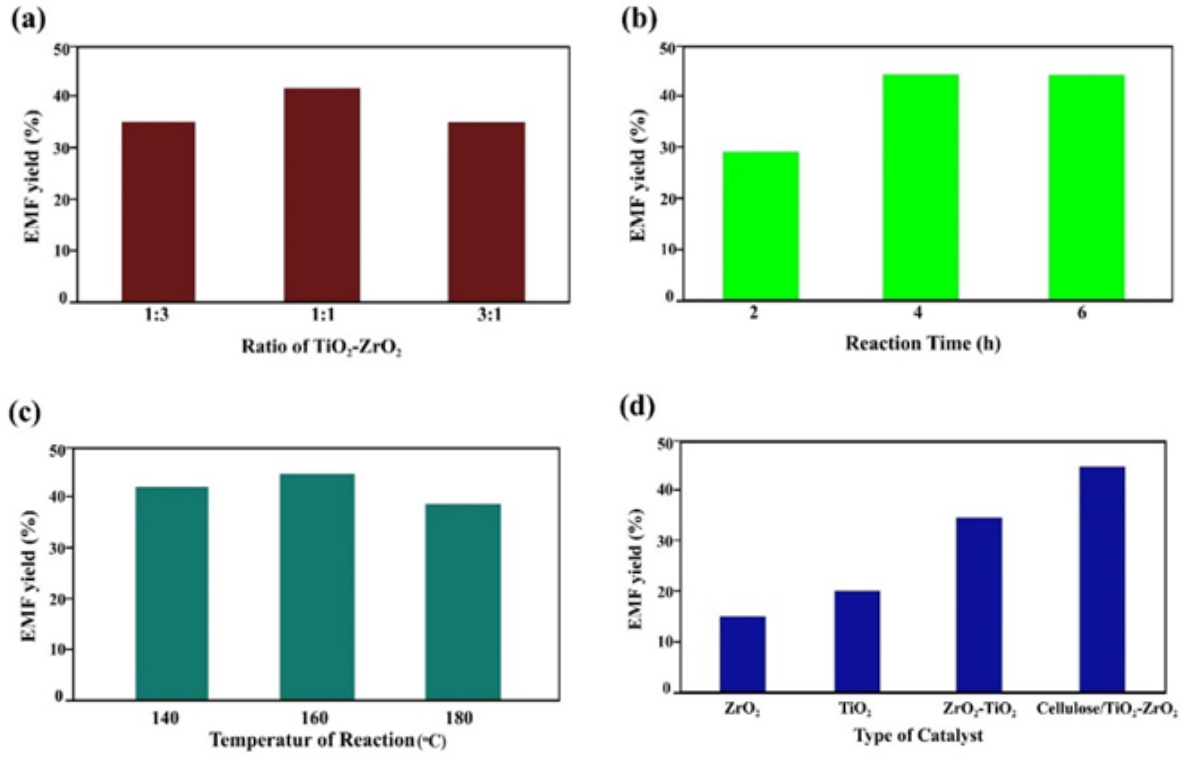

Figure 10. A variety of glucose conversions to 5-ethoxymethylfurfural: (a) ratio of TiO_2–ZrO_2 in a catalyst, (b) reaction time, (c) reaction temperature, and (d) type of catalyst.

TiO_2–ZrO_2, and cellulose–TiO_2–ZrO_2 achieved yields of 15.50%, 20.20%, 35.20%, and 45.50%, respectively (Figure 10d). The highest yield was observed for cellulose–TiO_2–ZrO_2, which was attributed to the synergetic effects of the hybridization of the biopolymer with inorganic nanoparticles [36].

We proposed a reaction mechanism for the catalytic activity of the cellulose–TiO_2–ZrO_2 catalyst in the reaction of glucose into 5-EMF (Figure 11). The first stage was isomerized into fructose compounds by Lewis acidic of TiO_2–ZrO_2 with the DMSO solvent and then the next stage by Brönsted acid derived from the sulfonate group of nanocelluloses into HMF. Furthermore, etherification of HMF into 5-EMF was synergistically catalyzed with a mixed binary oxide and nanocellulose catalyst.

4. Conclusion

In summary, we report a nanocomposite derived from sawdust cellulose combined with TiO_2–ZrO_2 binary oxide to form a cellulose–TiO_2–ZrO_2 nanocomposite, which can be utilized as a heterogeneous green catalyst for 5-EMF synthesis. This catalyst was shown to comprise porous and irregularly shaped TiO_2–ZrO_2 particles that are evenly distributed in the nanocellulose support. The presence of nanocellulose was important to increase the catalytic activity that induces the production of 5-EMF. Catalytic activity increased with the cellulose effect obtained ZrO_2, TiO_2, TiO_2–ZrO_2 and cellulose and TiO_2–ZrO_2 nanocomposite, with 15.50%, 20.20%, 35.20%, and 45.50% yields, respectively. The optimal yield of 5-EMF was 45.50%, with reaction conditions of 1:1 TiO_2–ZrO_2 ratio, 4 h reaction time, and 160 °C reaction temperature. The results suggested potential for using nanocellulose biopolymer from extracted from *Sengon* sawdust as a catalyst support material, which also increases the potential of renewable materials such as glucose to produce biofuel.

Acknowledgments

This research was supported by the Ministry of Research and Technology/National Research and Innovation through the PDUPT Grant No. NKB-170/UN2.RST/HKP.05.00/2021.

References

[1] Vallejos, M.E., Felissia, F.E., Area, M.C., Ehman, N.V., Tarrés, Q., Mutjé, P. (2016). Nanofibrillated cellulose (CNF) from eucalyptus sawdust as a dry strength agent of unrefined eucalyptus handsheets. *Carbohydrate Polymers*, 139, 99–105. DOI: 10.1016/j.carbpol.2015.12.004.

[2] Shaheen, T.I., Emam, H.E. (2018). Sonochemical synthesis of cellulose nanocrystals from wood sawdust using Acid hydrolysis. *International Journal of Biological Macromolecules*, 107(B), 1599–1606. DOI: 10.1016/j.ijbiomac.2017.10.028.

[3] Martinez Lopez, Y., Paes, J.B., Gustave, D., Gonçalves, F.G., Méndez, F.C., Theodoro Nantet, A.C. (2020). Production of wood-plastic composites using Cedrela odorata sawdust waste and recycled thermoplastics mixture from post-consumer products - A sustainable approach for cleaner production in Cuba. *Journal of Cleaner Production*, 244, 118723. DOI: 10.1016/j.jclepro.2019.118723.

[4] Trisnawati, L., Helmiyati, H. (2020). Cellulose-Fe3O4 nanocomposite based on rice husk as catalyst for synthesis of methyl ester from waste cooking oil. *IOP Conference Series: Materials Science and Engineering*, 763, 012012. DOI: 10.1088/1757-899X/763/1/012012.

[5] Helmiyati, H., Anggraini, Y. (2019). Nanocomposites comprising cellulose and nanomagnetite as heterogeneous catalysts for the synthesis of biodiesel from oleic acid. *International Journal of Technology*, 10(4), 798–807. DOI: 10.14716/ijtech.v10i4.2597.

[6] Azahra, S.N.A.R., Helmiyati, H. (2020). Synthesis of nanocomposites cellulose-Fe3O4/ZnO as novel green catalyst for biodiesel production from coconut oil. *IOP Conference Series: Materials Science and Engineering*, 959, 012016. DOI: 10.1088/1757-899X/959/1/012016.

[7] Ma, X., Liu, F., Helian, Y., Li, C., Wu, Z., Li, H., Chu, H., Wang, Y., Wang, Y., Lu, W., Guo, M., Yu, M., Zhou, S. (2021). Current application of MOFs based heterogeneous catalysts in catalyzing transesterification/esterification for biodiesel production: a review. *Energy Conversion and Management*, 229, 113760. DOI: 10.1016/j.enconman.2020.113760.

[8] Alipour, S., Omidvarborna, H., Kim, D.S. (2017). A review on synthesis of alkoxymethyl furfural, a biofuel candidate. *Renewable and Sustainable Energy Reviews*, 71, 908–926. DOI: 10.1016/j.rser.2016.12.118.

[9] Silahua-Pavón, A.A., Espinosa-González, C.G., Ortiz-Chi, F., Pacheco-Sosa, J.G., Pérez-Vidal, H., Arévalo-Pérez, J.C., Godavarthi, S., Torres-Torres, J.G. (2019). Production of 5-HMF from glucose using TiO2-ZrO2 catalysts: effect of the sol-gel synthesis additive. *Catalysis Communications*, 129, 105723. DOI: 10.1016/j.catcom.2019.105723.

[10] He, R., Huang, X., Zhao, P., Han, B., Wu, T., Wu, Y. (2018). The synthesis of 5-hydroxymethylfurfural from glucose in biphasic system by phosphotungstic acidified titanium–zirconium dioxide. *Waste and Biomass Valorization*, 9(4), 657–668. DOI: 10.1007/s12649-017-0024-9.

[11] Kargarzadeh, H., Johar, N., Ahmad, I. (2017). Starch biocomposite film reinforced by multiscale rice husk fiber. *Composites Science and Technology*, 151, 147–155. DOI: 10.1016/j.compscitech.2017.08.018.

[12] Jiang, F., Kondo, T., Hsieh, Y.-L. (2016). Rice straw cellulose nanofibrils via aqueous counter collision and differential centrifugation and their self-assembled structures. *ACS Sustainable Chemistry and Engineering*, 4(3), 1697–1706. DOI: 10.1021/acssuschemeng.5b01653.

[13] Helmiyati, H., Masriah, I. (2019). Preparation of cellulose/CaO-Fe_2O_3 nanocomposites as catalyst for fatty acid methyl ester production. *AIP Conference Proceedings*, 2168, 020062. DOI: 10.1063/1.5132489.

[14] Kumar, T.S.M., Rajini, N., Reddy, K.O., Rajulu, A.V., Siengchin, S., Ayrilmis, N. (2018). All-cellulose composite films with cellulose matrix and Napier grass cellulose fibril fillers. *International Journal of Biological Macromolecules*, 112, 1310–1315. DOI: 10.1016/j.ijbiomac.2018.01.167.

[15] Prado, K.S., Spinacé, M.A.S. (2019). Isolation and characterization of cellulose nanocrystals from pineapple crown waste and their potential uses. *International Journal of Biological Macromolecules*, 122, 410–416. DOI: 10.1016/j.ijbiomac.2018.10.187.

[16] Liu, C., Li, B., Du, H., Lv, D., Zhang, Y., Yu, G., Mu, X., Peng, H. (2016). Properties of nanocellulose isolated from corncob residue using sulfuric acid, formic acid, oxidative and mechanical methods. *Carbohydrate Polymers*, 151, 716–724. DOI: 10.1016/j.carbpol.2016.06.025.

[17] Zhang, J., Li, L., Li, Y., Yang, C. (2017). Microwave-assisted synthesis of hierarchical mesoporous Nano-TiO_2/cellulose composites for rapid adsorption of Pb^{2+}. *Chemical Engineering Journal*, 313, 1132–1141. DOI: 10.1016/j.cej.2016.11.007.

[18] Grządka, E., Matusiak, J. (2020). Changes in the CMC/ZrO_2 system properties in the presence of hydrocarbon, fluorocarbon and silicone surfactants. *Journal of Molecular Liquids*, 303, 112699. DOI: 10.1016/j.molliq.2020.112699.

[19] Maleki, A., Jafari, A.A., Yousefi, S. (2017). Green cellulose-based nanocomposite catalyst: design and facile performance in aqueous synthesis of pyranopyrimidines and pyrazolopyranopyrimidines. *Carbohydrate Polymers*, 175, 409–416. DOI: 10.1016/j.carbpol.2017.08.019.

[20] Helmiyati, H., Dini, F.W. (2018). Synthesis and application of nanocomposite based on Nano sodium alginate from brown seaweed impregnation TiO_2 as a catalyst for synthesis 5-hydroxymethylfurfural from fructose. *AIP Conference Proceedings*, 2023, 020101. DOI: 10.1063/1.5064098.

[21] Lestari, I., Helmiyati, H. (2020). Calcium alginate-TiO_2/SiO_2 nanocomposite for glucose conversion to 5-hydroxymethylfurfural. *IOP Conference Series: Materials Science and Engineering*, 763, 012037. DOI: 10.1088/1757-899X/763/1/012037.

[22] Helmiyati, H., Abbas, G.H., Budiman, Y., Ramadhani, S. (2020). Synthesis of $MgFe_2O_4$-MgO nanocomposite: influence of MgO on the catalytic activity of magnesium ferrite in biodiesel production. *Rasayan Journal of Chemistry*, 13(1), 298–305. DOI: 10.31788/RJC.2020.1315497.

[23] Zuo, M., Jia, W., Feng, Y., Zeng, X., Tang, X., Sun, Y., Lin, L. (2021). Effective selectivity conversion of glucose to furan chemicals in the aqueous deep eutectic solvent. *Renewable Energy*, 164, 23–33. DOI: 10.1016/j.renene.2020.09.019.

[24] Zhang, J., Dong, K., Luo, W., Guan, H. (2018). Catalytic upgrading of carbohydrates into 5-ethoxymethylfurfural using SO3H functionalized hyper-cross-linked polymer based carbonaceous materials. *Fuel*, 234, 664–673. DOI: 10.1016/j.fuel.2018.07.060.

[25] Chen, B., Yan, G., Chen, G., Feng, Y., Zeng, X., Sun, Y., Tang, X., Lei, T., Lin, L. (2020). Recent progress in the development of advanced biofuel 5-ethoxymethylfurfural. *BMC Energy*, 2(1), 1–13. DOI: 10.1186/s42500-020-00012-5.

[26] Mushtaq, K., Saeed, M., Gul, W., Munir, M., Firdous, A., Yousaf, T., Khan, K., Sarwar, H.M.R., Riaz, M.A., Zahid, S. (2020). Synthesis and characterization of TiO_2 via sol-gel method for efficient photocatalytic degradation of antibiotic ofloxacin. *Inorganic and Nano-Metal Chemistry*, 50(7), 580–586. DOI: 10.1080/24701556.2020.1722695.

[27] Chintaparty, C.R. (2016). Influence of calcination temperature on structural, optical, dielectric properties of Nano zirconium oxide. *Optik*, 127(11), 4889–4893. DOI: 10.1016/j.ijleo.2016.02.014.

[28] Kambur, A., Pozan, G.S., Boz, I. (2012). Preparation, characterization and photocatalytic activity of TiO_2-ZrO_2 binary oxide nanoparticles. *Applied Catalysis B*, 115–116, 149–158. DOI: 10.1016/j.apcatb.2011.12.012.

[29] Kanakaraju, D., Ravichandar, S., Lim, Y.C. (2017). Combined effects of adsorption and photocatalysis by hybrid TiO_2/ZnO-calcium alginate beads for the removal of copper. *Journal of Environmental Sciences (China)*, 55, 214–223. DOI: 10.1016/j.jes.2016.05.043.

[30] Chen, T., Peng, L., Yu, X., He, L. (2018). Magnetically recyclable cellulose-derived carbonaceous solid acid catalyzed the biofuel 5-ethoxymethylfurfural synthesis from renewable carbohydrates. *Fuel*, *219*, 344–352. DOI: 10.1016/j.fuel.2018.01.129.

[31] Zuo, M., Le, K., Feng, Y., Xiong, C., Li, Z., Zeng, X., Tang, X., Sun, Y., Lin, L. (2018). An effective pathway for converting carbohydrates to biofuel 5-ethoxymethylfurfural via 5-hydroxymethylfurfural with deep eutectic solvents (DESs). *Industrial Crops and Products*, 112, 18–23. DOI: 10.1016/j.indcrop.2017.11.001.

[32] Helmiyati, H., Fitriyani, A., Meyanti, F. (2017). The copolimeryzation synthesis and swelling capacity of cellulose-poly superabsorbent (acrylic acid-co-acrylamide) based on rice straw. *IOP Conference Series: Materials Science and Engineering*, 188, 012051. DOI: 10.1088/1757-899X/188/1/012051.

[33] Helmiyati, H., Suci, R.P. (2019). Nanocomposite of cellulose-ZnO/SiO2 as catalyst biodiesel methyl ester from virgin coconut oil. *AIP Conference Proceedings*, 2168, 020063. DOI: 10.1063/1.5132490.

[34] Bauli, C.R., Rocha, D.B., de Oliveira, S.A., Rosa, D.S. (2019). Cellulose nanostructures from wood waste with low input consumption. *Journal of Cleaner Production*, 211, 408–416. DOI: 10.1016/j.jclepro.2018.11.099.

[35] Martakov, I.S., Torlopov, M.A., Mikhaylov, V.I., Krivoshapkina, E.F., Silant'ev, V.E., Krivoshapkin, P.V. (2018). Interaction of cellulose nanocrystals with titanium dioxide and peculiarities of hybrid structures formation. *Journal of Sol-Gel Science and Technology*, 88, 13–21. DOI: 10.1007/s10971-017-4447-3.

[36] Gong, J., Katz, M.J., Kerton, F.M. (2018). Catalytic conversion of glucose to 5-hydroxymethylfurfural using zirconium-containing metal-organic frameworks using microwave heating. *RSC Advances*, 8(55), 31618–31627. DOI: 10.1039/C8RA06021E.

Selected and Revised Papers from 3rd International Conference on Chemistry, Chemical Process and Engineering 2020 (IC3PE 2020) (https://chemistry.uii.ac.id/ic3pe/) (Universitas Islam Indonesia (UII), Labuan Bajo, Nusa Tenggara Timur, Indonesia by 30th September – 1st October 2020) after Peer-reviewed by Scientific Committee of IC3PE 2020 and Peer-Reviewers of Bulletin of Chemical Reaction Engineering & Catalysis. Editors: Is Fatimah, I. Istadi.